IEEE Access
Multidisciplinary | Rapid Review | Open Access Journal

Received August 12, 2021, accepted August 24, 2021, date of publication September 3, 2021, date of current version September 15, 2021.

Digital Object Identifier 10.1109/ACCESS.2021.3109974

Design, Analysis, and Implementation of a Four-DoF Chair Motion Mechanism

MING-YEN WEI[1], YEN-LIANG YEH[2], SHIAW-WU CHEN[3], HSIU-MING WU[4], AND JI-WEI LIU[1]

[1]Aeronautical System Research Division, Simulation System Section, National Chung-Shan Institute of Science and Technology, Taichung 407, Taiwan
[2]Department of Mechanical Engineering, National Chin-Yi University of Technology, Taichung 411, Taiwan
[3]Department of Automatic Control Engineering, Feng Chia University, Taichung 407, Taiwan
[4]Department of Intelligent Automation Engineering, National Taipei University of Technology, Taipei 106, Taiwan

Corresponding author: Ming-Yen Wei (tim583980@gmail.com)

This work was supported by the National Chin-Yi University of Technology, Taiwan, under Grant NCUT 19-T-EM-055.

ABSTRACT In this study, the proposed design of a motion chair with four degrees of freedom (DoF) provides the pilot with the tactile sensations required by the human body to increase the immersion of flight simulation training. The chair includes a seat pan, a back pad, and a seat height. For the development of the proposed mechanism structure, the modular design is used to achieve the required displacement and acceleration. In addition, inverse kinematics is also constructed to meet the actuation needs. The control system can achieve real-time closed-loop control using an industrial computer, a motion control card, servo motors and drivers. This enables the structure to reach destinations with the shortest motion time and completes the required T-curve motion trajectory. The displacement, velocity, and acceleration of the designed structure are analyzed using SimWise4D software to verify the performance specifications of the structure. The experimental results indicate that the four-DoF control meets requirements of displacement, velocity, and acceleration.

INDEX TERMS Motion chair, mechatronics, kinematics, motion analysis.

I. INTRODUCTION

The training of pilots worldwide is typically lengthy. Therefore, flight training simulators are in high demand and serve as essential tools in flight training. As indicated in [1], a complete high fidelity motion simulation system was first constructed in the 1950s. In 1954, the General Precision Corporation of United States developed a motion simulation system that performed 3° pitching, rolling, and yawing. After continual improvements, the system performed 10° pitching, rolling, and yawing by 1964. In 1965, Stewart proposed the six-axis parallel motion platform structure [2]. In 1969, the hydraulic driver of a civil aviation simulator controlled the motion of each axis, which meant that it possessed six DoF. Thus, the basic design framework of the simulator was established in [3]. The contact sensations of the human body differ from the spatial sensations generated by the six-DoF platform. Subsequently, many studies explored and improved the framework, including discussion on identifying the relationships of six-axis motion and each actuator through kinematics [4] and discussion on how the disturbance rate of the compensation load could enhance positioning precision [5].

However, the oppressive sensation generated by gravity on human body can be provided by contact with the motion chair. In a study conducted by Gum [6], the testing of a research model indicated the presence of a time delay between the applied force and the perception of various mechanisms. Intramuscular and pressure detection structures perceived applied force at a faster rate than the vestibular system did. In 1976, Cardullo and Harpursville [7] engaged in chair design with the hope of using a chair to stimulate the tactile sensory system. They hoped that the seat would independently produce the expected skeletal posture changes, simulate regions related to skin contact changes, and reflect variation in the muscular pressure gradient. They also aimed to simulate the effect of acceleration. The chair contains two airbags, which form the seat and Back pads. Therefore, the control method could be used to independently drive the airbags in order to manipulate the height, position, and shape of the support surface. In the design, the tactile sensation of the body surface is altered using changes in airbags. In 2007, Berger *et al.* performed a study on perceptions and visual sensations [8] and indicated that

The associate editor coordinating the review of this manuscript and approving it for publication was Tao Wang.

qualitative matching between the perception and the size of visual acceleration could enhance the information transmission between them. The results indicated that the use of visual effects in the construction of a motion notification warning algorithm could enhance the linear acceleration motion effect of the simulator. In [9], Bruschetta *et al.* used the Stewart platform in conjunction with a seat in a motion platform. Specifically, the researchers created the feeling of continuous low-frequency acceleration by placing eight inflators on the chair. Four were placed on chair's back, two on the seat pan, and one on either side of the safety belt. The devices created the feeling of continuous low-frequency acceleration through the sense of restraint imposed by the safety belt after the devices inflate. In [10], the researchers designed a single DoF seat simulator to examine the fatigue the body perceived after prolonged driving. The simulator comprised a one-DoF chair, steering wheel, and visual effects and tested the body's level of fatigue through the adjustment of a surge axis on the back. In [11], a two-DoF (roll and pitch axis) seat was developed. The researchers used the seat rolling and the surge axis rotation to test whether automated cars would be able to predict the position and behaviors of other cars after 3 seconds. In [12], a shaker rig was designed based on linear servomotors for testing ride comfort drivers perceived.

The majority of simulators have been designed based on the six-DoF structure of the Stewart platform [13]–[15], which simulates and presents a six-DoF overall movement. However, the Stewart platform is unable to simulate the kinematic sensations that a pilot experiences when flying. Therefore, this work proposes a four- DoF chair system for motion simulation. The system consists of a gravity chair that provides the user with somatosensory sensations. The purpose of the system is to provide pilots with tactile sensations related to motion. The bodily sensations that pilots experience while flying are converted into data. This enables pilots to experience relevant tactile sensations and makes flight simulation a more immersive experience. The design, analysis, and control of the chair are conducted based on mathematical model construction. The kinematic models are employed to describe the relationship between the movement position of the simulator in space and the rotating angles of each joint, in structure analysis, and to understand the limitations of the motion space. The seat pan component consists of a heave axis structure and a roll axis structure. The back pad component comprises a sway axis structure and a surge axis structure. The seat height structure consists of a whole-chair adjustable vertical structure. Because each component has a single level of motion DoF, the researchers refer to the method used in [16]–[18] and identified inverse kinematic model based on the geometrical relationship between the connecting rods. By contrast, inverse kinematics involves obtaining the displacement or angles of each joint based on reverse engineering of the movement position and attitude of the simulator in space.

Generally speaking, it is very difficult to use the Stewart platform to train pilots as a simulator, especially for the sense of gravity in a short distance movement. The paper proposes a four-DoF chair as the gravity motion needed for flight. To the best of our knowledge, the ideas we mentioned have not been presented in the previously published papers [1]–[18]. As a result, this paper presents some new ideas in the implementation of motion chair control systems, including an adjustable speed control system and short distance stroke control system.

II. KINEMATIC MODEL

The structure of the motion chair contains three components shown in Fig. 1. The seat pan component is composed of the roll and heave structures. The chair's back pad component is composed of the surge and sway structures. The seat height structure of the whole chair is composed of the whole-chair adjustable height structure. As shown in Figure 1, it includes a pilot and the direction of three coordinate axes.

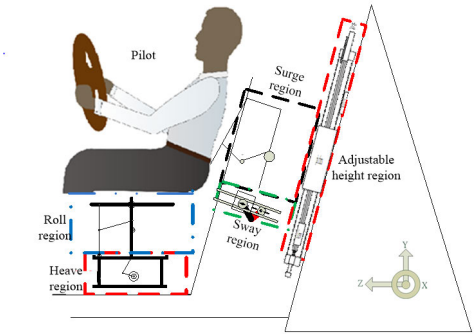

FIGURE 1. The schematic diagram of the designed motion chair.

A. KINEMATICS OF THE SEAT PAN

1) INVERSE KINEMATICS OF THE ROLL AXIS

The roll structure of the seating plate is the toggle joint structure shown in Fig. 2. In Fig. 2, l_2, l_3, l_4, l_5, l_6 represent the lengths of the links, in which l_6 is the length of the seat, l_4 denotes the length of the driving link, l, l_0, l_1 represent the distances between rotation axes and l_0 and l_1 are the known terms. The constraint equations have to satisfy geometric

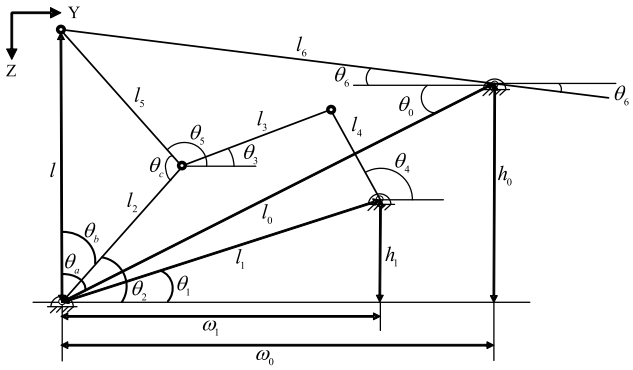

FIGURE 2. The schematic diagram of the seat plate rolling mechanism.

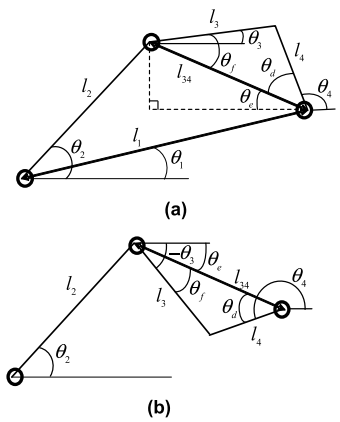

FIGURE 3. Two solutions of θ_3 and θ_4: (a) solution1 (2) solution2.

relationship in Eqs. (1)-(4).

$$l_2\cos\theta_2 + l_3\cos\theta_3 - l_4\cos\theta_4 - \omega_1 = 0 \tag{1}$$

$$l_2\sin\theta_2 + l_3\sin\theta_3 - l_4\sin\theta_4 - h_1 = 0 \tag{2}$$

$$l_4\cos\theta_4 - l_3\cos\theta_3 + l_5\cos\theta_5 + l_6\cos\theta_6 - (\omega_0 - \omega_1) = 0 \tag{3}$$

$$l_4\sin\theta_4 - l_3\sin\theta_3 + l_5\sin\theta_5 - l_6\sin\theta_6 - (h_0 - h_1) = 0 \tag{4}$$

For the inverse kinematics of the roll axis, the angles of each link from θ_6 and the turning angle of the seating plate must be obtained. First, θ_2 is determined and then followed by solving for l based on θ_0 and l_0 as follows:

$$\theta_0 = \tan^{-1}\frac{h_0}{\omega_0} \tag{5}$$

$$l_0 = \sqrt{h_0^2 + \omega_0^2} \tag{6}$$

$$l = \sqrt{l_0^2 + l_6^2 - 2l_0^2 l_6^2\cos(\theta_0 + \theta_6)} \tag{7}$$

Subsequently, θ_a can be obtained based on l, l_0, and l_6

$$\frac{l_6}{\sin\theta_a} = \frac{l}{\sin(\theta_0 + \theta_6)} \tag{8}$$

We can derive

$$\theta_a = \sin^{-1}\left(\frac{l_6}{l}\sin(\theta_0 + \theta_6)\right) \tag{9}$$

Based on l, l_2, and l_5, θ_b can be obtained as

$$\theta_b = \cos^{-1}\left(\frac{l_2^2 + l^2 - l_5^2}{2l_2 l}\right) \tag{10}$$

θ_2 can be calculated and given as

$$\theta_2 = \theta_a + \theta_0 - \theta_b \tag{11}$$

For the next step, θ_3 and θ_4 are solved. As shown in Figs. 3(a)-(b), there are two solutions for θ_3 and θ_4.

According to Fig. 2 and Fig. 3(a), the solution 1 can obtain θ_3. Next, l_{34} must be first solved and expressed as

$$\theta_1 = \tan^{-1}\frac{h_1}{\omega_1} \tag{12}$$

$$l_1 = \sqrt{h_1^2 + \omega_1^2} \tag{13}$$

$$l_{34} = \sqrt{l_1^2 + l_2^2 - 2l_1^2 l_2^2\cos(\theta_2 - \theta_1)} \tag{14}$$

Then, θ_f can be obtained from l_{34}, l_3, and l_4,

$$\theta_f = \cos^{-1}\frac{l_3^2 + l_{34}^2 - l_4^2}{2l_{34}l_3} \tag{15}$$

According Fig. 2, θ_e can be expressed as

$$\theta_e = \tan^{-1}\frac{l_2\sin\theta_2 - h_1}{\omega_1 - l_2\cos\theta_2} \tag{16}$$

From Eqs. (15)-(16), θ_3 can be obtained

$$\theta_3 = \theta_f - \theta_e \tag{17}$$

Similarly, θ_d can be obtained from l_{34}, l_3, and l_4, and then θ_4 can be calculated as

$$\theta_d = \cos^{-1}\frac{l_4^2 + l_{34}^2 - l_3^2}{2l_4 l_{34}} \tag{18}$$

$$\theta_4 = 180 - \theta_d - \theta_e \tag{19}$$

Fig. 3(b) is the other solution for θ_3 and θ_4,

$$\theta_3 = -\theta_f - \theta_e \tag{20}$$

$$\theta_4 = 180 + \theta_d - \theta_e \tag{21}$$

The next step involves solving for θ_5. Given that $l_3 + l_4 < \omega_1$, there is only one solution for θ_2 and θ_5. Based on the following figure, θ_c can be obtained based on l, l_2, and l_5, whereas θ_5 can be obtained based on θ_c and θ_2,

$$\theta_c = \cos^{-1}\frac{l_2^2 + l_5^2 - l^2}{2l_2 l_5} \tag{22}$$

$$\theta_5 = 180 - (\theta_c - \theta_2) \tag{23}$$

According to Eqs. (11), (17), (20), (21) and (23), the link angles can be obtained as control commands and then achieve the seating plate control of the roll region.

2) INVERSE KINEMATICS OF THE HEAVE AXIS

The seating place structure of the heave axis is designed as the slider crank mechanism shown in Fig. 4. The mechanism is similar to a press machine as [17], [18]. In Fig. 4, l_8 represents the driving link; l_7 denotes the initial height of the seating plate; and z stands for the seating plate's displacement. The

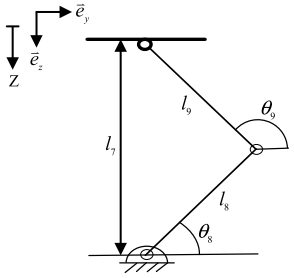

FIGURE 4. The diagram of the seating place heave mechanism.

displacement and the angles of each link must satisfy constraints of Eqs. (24)-(25).

$$l_7 - z = l_8 \sin\theta_8 + l_9 \sin\theta_9 \tag{24}$$
$$l_8 \cos\theta_8 + l_9 \cos\theta_9 = 0 \tag{25}$$

Inverse kinematics of the heave axis and angles of each link from z-axis displacement of the seating plate must be first obtained. As shown in the Figs. 5(a) and (b), there are two solutions for this relationship.

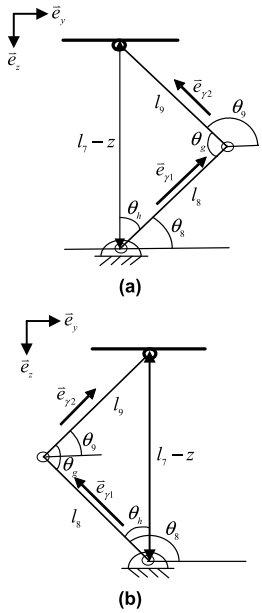

FIGURE 5. Two solutions of θ_8 and θ_9: (a) solution1 (2) solution2.

According to Fig. 5(a), the solution 1 obtains θ_g and θ_h, z, l_8 and l_9 must be first solved and expressed as

$$\theta_g = \cos^{-1}\frac{l_8^2 + l_9^2 - (l_7 - z)^2}{2l_8 l_9} \tag{26}$$
$$\theta_h = \cos^{-1}\frac{(l_7 - z)^2 + l_8^2 - l_9^2}{2l_8\,(l_7 - z)} \tag{27}$$

Next, θ_8 and θ_9 can be obtained as

$$\theta_8 = 90 - \theta_h \tag{28}$$
$$\theta_9 = 180 - (\theta_g - \theta_8) \tag{29}$$

Fig. 5(b) is the other solution for θ_8 and θ_9,

$$\theta_8 = \theta_h + 90 \tag{30}$$
$$\theta_9 = \theta_g - (180 - \theta_8) \tag{31}$$

By combining (30) and (31), we can obtain

$$\theta_9 = \theta_g + \theta_h - 90 \tag{32}$$

From observation, the link angles (30), (32) can be obtained as control commands and further attain the seating place control of the heave region.

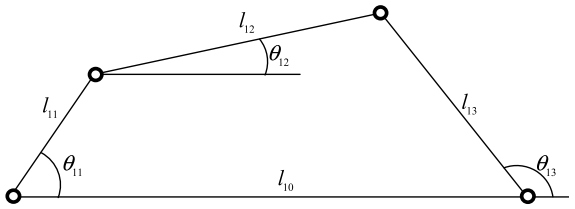

FIGURE 6. The schematic diagram of the four-link mechanism.

B. KINEMATICS OF THE BACK PAD

1) INVERSE KINEMATICS OF THE SURGE AXIS

As shown in Fig. 6, a four-link mechanism is used for the surge axis structure of the chair's back. In Fig. 6, l_{11} represents the driving link and l_{13} represents the chair's back. The angles of each link must satisfy Eqs. (33)-(34).

$$l_{11}\cos\theta_{11} + l_{12}\cos\theta_{12} - l_{13}\cos\theta_{13} - l_{10} = 0 \tag{33}$$
$$l_{11}\cos\theta_{11} + l_{12}\sin\theta_{12} - l_{13}\sin\theta_{13} = 0 \tag{34}$$

The surge axis's inverse kinematics involves obtaining θ_{11} and θ_{12} from the turning angle and θ_{13} of the rear panel. In Figs. 7(a) and (b), there are two solutions with the collinear boundaries of links l_{11} and l_{12}.

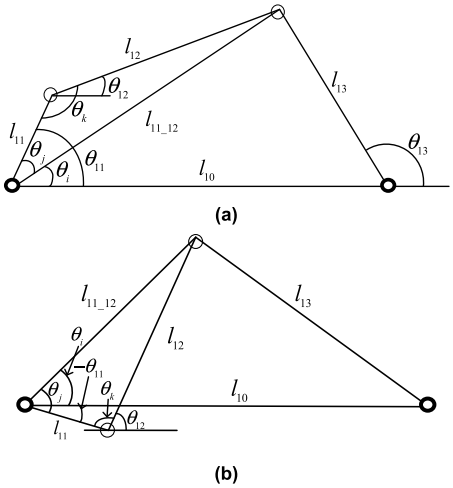

FIGURE 7. Two solutions of θ_{11} and θ_{12}: (a) solution1 (2) solution2.

According to Fig. 7(a), the solution 1 obtaining from l_{11_12}, l_{10}, l_{13} and θ_{13} must be first solved and expressed as

$$\begin{aligned} l_{11\_12} &= l_{10}^2 + l_{13}^2 - 2l_{10}l_{13}\,(180 - \theta_{13}) \\ &= l_{10}^2 + l_{13}^2 + 2l_{10}l_{13}\,(\theta_{13}) \end{aligned} \tag{35}$$

Next, θ_{11} and θ_{12} can be obtained based on θ_i, θ_j, and θ_k as follows:

$$\theta_i = \cos^{-1}\frac{l_{10}^2 + l_{11\_12}^2 - l_{13}^2}{2l_{10}l_{11\_12}} \tag{36}$$
$$\theta_j = \cos^{-1}\frac{l_{11}^2 + l_{11\_12}^2 - l_{12}^2}{2l_{11}l_{11\_12}} \tag{37}$$

$$\theta_k = \cos^{-1}\frac{l_{11}^2 + l_{12}^2 - l_{11\_12}^2}{2l_{11}l_{12}} \quad (38)$$

$$\theta_{11} = \theta_i + \theta_j \quad (39)$$

$$\theta_{12} = \theta_k - (180 - \theta_{11}) \quad (40)$$

Fig. 7(b) is the other solution. θ_i, θ_j, and θ_k can be solved using the same method. Then, θ_{11} and θ_{12} can be solved as

$$\theta_{11} = \theta_i - \theta_j \quad (41)$$

$$\theta_{12} = 180 - (\theta_k - \theta_{11}) \quad (42)$$

From Eqs. (39)–(42) the angles of each link can be obtained as control commands. Subsequently, the real panel control of the surge region is achieved.

2) INVERSE KINEMATICS OF THE SWAY AXIS

Similarly, the sway axis structure of the back pad is the same with the heave axis. Both of them are designed as the slider crank mechanism shown in Fig. 4. Therefore, Eqs. (30) and (32) can be obtained by using the same derivation

C. KINEMATICS OF THE SEAT HEIGHT

In this section, ball screw is used for the adjustable height structure of the whole chair. Assuming that the lead of the ball screw is D (m/rev), then the relationship between displacement H and rotating angle θ_{14} is

$$H = \frac{D}{2\pi}\theta_{14} \quad (43)$$

D. SIMULATION VERIFICATION

To verify the correctness of the above-mentioned inverse kinematics, the simulation verification for the kinematics of the seating plate roll axis structure is performed using Matlab. The structure's dimensions in the simulation are $l_2 = 10$mm, $l_3 = 180$mm, $l_4 = 3$mm, $l_5 = 10$mm, $l_6 = 22.5$mm, $h_0 = 16$mm, $h_1 = 4.5$mm and $\omega_0 = \omega_1 = 22.5$mm. With regard to the kinematic equations, θ_2, θ_3, and θ_4 can be solved using θ_6, and the verification process can be conducted by substituting them into Eqs. (1)–(4). The obtained error is within the range of 10^{-13} to 10^{-15}. The dimensions of the seating place heave structure used in the simulation are $l_7 = 70$mm, $l_8 = 3$mm and $l_9 = 70$mm. With regard to the inverse kinematic equations, θ_8 and θ_9 can be solved using z, and the verification can be conducted by substituting them into Eqs. (24)–(25). The result is that the obtained error is within the range of 10^{-13} to 10^{-15}. For the kinematics of the chair's back surge axis structure, the dimensions are $l_{10} = 388.5$mm, $l_{11} = 52.5$mm, $l_{12} = 192.2$mm, $l_{13} = 224$mm. The program is first executed the inverse kinematics equations in the subsection B part of section II part, and solved for θ_{11} and θ_{12} based on θ_{13}. The verification could then be conducted by substituting them into Eqs. (33)–(34). The obtained error is within the range of 10^{-13} to 10^{-15}. The sway axis structure of the back pad is the same as the heave axis. The dimensions used in the simulation are $l_7 = 75$mm, $l_8 = 15$mm and $l_9 = 75$mm. The obtained error of the simulation verification is within the range of 10^{-13} to 10^{-15}. From Eq. (43), we can observe that the kinematic model of the seat height is fairly simple. Hence, its verification is omitted here.

III. DESIGN AND ANALYSIS OF THE MOTION CHAIR

This section is divided into five regions. First, the design of the seat pan is mainly based on the roll-axis region and heave-axis region. Next, the design of the back pad is mainly based on the surge-axis region and sway-axis region. Finally, the seat height is designed so that the height of the entire seat is adjustable. In order to effectively verify the displacement, speed and acceleration of this designed mechanism, the SimWise 4D software is used to analyze the displacement, speed and acceleration of the mechanism. The CAD modeling of the work is constructed by the Solidworks software. Then, the solid modeling of the chair is inputted the SimWise 4D software to simulate the dynamic motion of the chair. The SimWise 4D is the mechanical software. SimWise 4D is for design and engineering professionals developing products involving assemblies of 3D parts [19].

A. SEAT PAN MECHANISM

1) MECHANISM DESIGN

According to Fig. 1, the roll region is the rotating chair base with a dual base plate. Fixed phase differences exist for the motion of the dual base plate. The design of the dual base plate is a design of 180° such that the single DoF on one side can be extended to the other side to execute the roll motion. The structure is designed to sustain the weight of a human body and the weight of the chair surface. Thus, a toggle joint structure module design is used. The size of the chair is 600 mm * 560 mm as shown in Fig. 8. Figures 9(a) and (b) respectively represent schematics of the platform surface and the supporting frame.

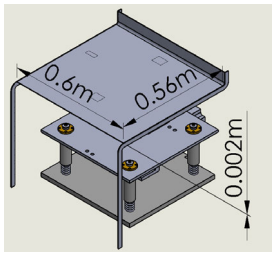

FIGURE 8. Chair dimensions.

The roll axis has to generate a rolling effect on the seat pan with a larger force required to be exerted larger body mass. Hence, a toggle structure is used for the design as shown in Figs. 10(a), (b), and (c). The structure length is 249.42 mm. As shown in Figs. 11(a) and (b), the design of the heave axis involves a combination of eccentricity and link.

2) ANALYSIS OF THE MECHANISM

The displacement, velocity, and acceleration of the seat's base may be analyzed assuming that the roll axis motor rotates at a speed of 300 rpm. The results are shown in

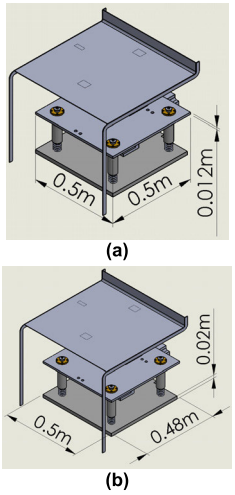

FIGURE 9. Dimensions of heave axis, (a) platform surface and (b) supporting frame.

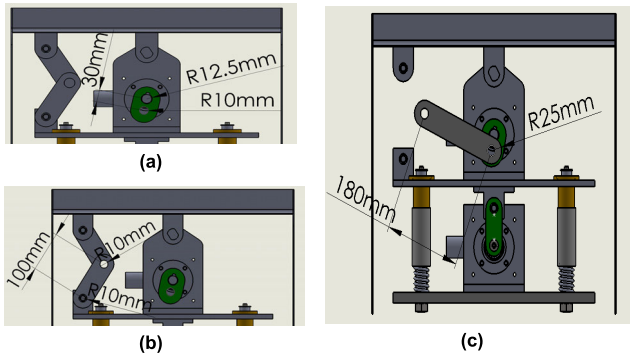

FIGURE 10. Design of the roll axis structure, (a) dimensions of the crank shaft, (b) dimensions of the structure's toggle and two-bar linkage (c) dimensions of the structure's toggle and two-bar linkage.

Figs. 12(a), (b), and (c), respectively. It is observed that the maximum displacement is 0.515-0.431 = 0.084m, the position is ±0.042m. The speed is 1.53-(-1.33) = 2.86m/s, and the speed is ±1.43 m/s. The peak to peak acceleration is 62.3-(-38.2) = 100.5m/s^2, or the averaged acceleration is ±50.25m/s^2.

Assuming that the heave axis motor rotates at a speed of 300 rpm but the roll axis motor is still, the displacement, velocity, and acceleration of the chair's base are analyzed, the results are shown in Figs. 13(a), (b), and (c), respectively. Then the maximum displacement is 0.481-0.475 = 0.006m and the position is ±0.003m. The speed is 0.0908-(-0.0908) = 0.1816m/s, and the speed is ±0.0908 m/s. The peak to peak acceleration is 2.83-(-3.09) = 5.92m/s^2, or it can be said that the averaged acceleration is ±2.96m/s^2.

B. BACK PAD MECHANISM

1) MECHANISM DESIGN

The surge and sway regions are shown in Fig. 1. A design for surge is based on the design of rotary vanes. The main mechanism involves driving using a four-bar linkage such that

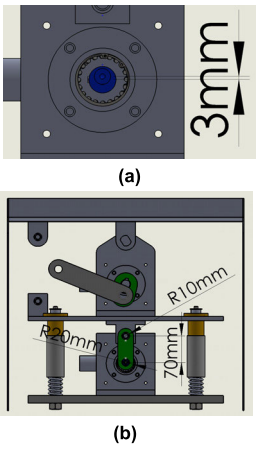

FIGURE 11. Dimensions of heave axis, (a) platform surface and (b) supporting frame.

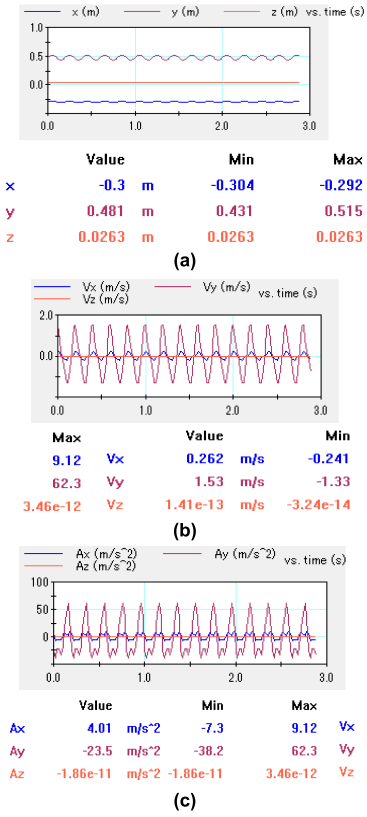

FIGURE 12. Measurement and analysis of the roll axis, (a) displacement, (b) velocity and (c) acceleration.

the structure is actuated within a small space. On the other hand, the sway makes use of a four-bar linkage crank sliding structure and generates a movement rate of ±15 mm through the design of the crank shaft length. In addition, the chair's back motion contains both surge and sway motion. Therefore, the mechanism design requires two motors to drive surge axis and sway axis. Figures 14 and 15 respectively show the dimensions of the supporting platform surface and the contact surface between the back pad and the chair's back.

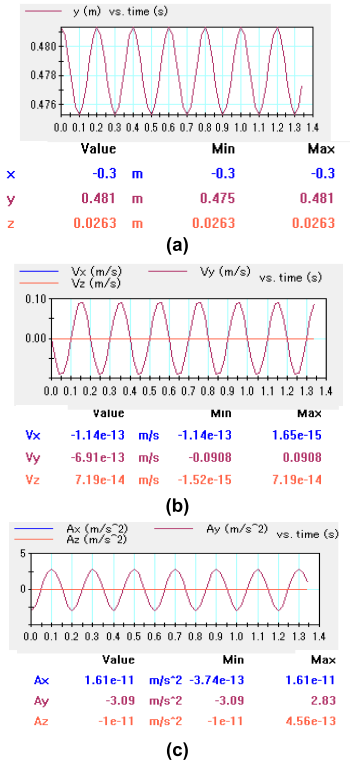

FIGURE 13. Measurement and analysis of the heave axis, (a) displacement, (b) velocity and (c) acceleration.

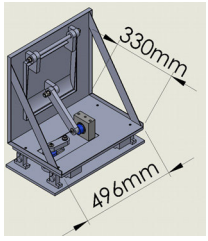

FIGURE 14. Dimensions of the back pad's supporting platform surface.

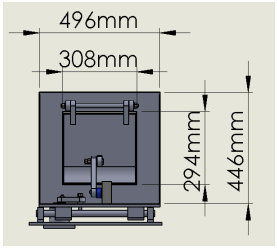

FIGURE 15. Dimensions of the contact surface between the back pad and the chair's back.

The design of the surge axis is based on rotary vanes such that the structure could be actuated within a small space. The main mechanism involves driving a four-bar linkage using a motor. The structure requires a small space and the required force exertion is not large. Figure 16 illustrates the eccentricity of the crank shaft. The sway axis motion mainly depends

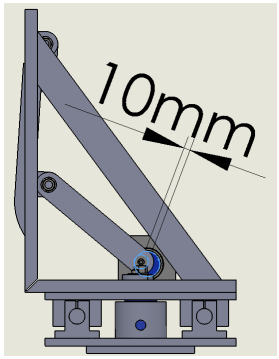

FIGURE 16. Eccentricity of the surge axis's crank shaft.

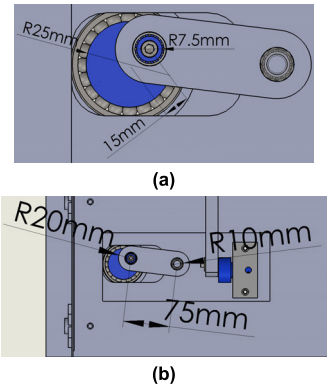

FIGURE 17. Design of the sway axis structure, (a) crank and (b) link.

on the structure of the chair's back. Therefore, the focus of the designed planning is on the crank–slider structure of a four-bar linkage. The dimensions of the crank and the link are shown in Figs. 17 (a) and (b).

2) ANALYSIS OF MECHANISM

At a rotating speed of 300 rpm, the surge and sway directions of the chair's back are analyzed. The results are shown in Fig. 18 and Fig. 19, respectively. In Fig. 18(a), the maximum displacement is 0.032-0.0144 = 0.176m and the position is ±0.0088m. The speed in Fig. 18(b) is 0.277-(-0.294) = 0.571 m/s and the speed is ±0.285m/s. The acceleration in Fig. 18(c) is 9.24(-8.54) = 17.78m/s^2 and the acceleration is ±8.89m/s^2. In Fig. 19(a), the maximum displacement is 0.000281-0.0297 = 0.029981m and the position is ±0.01488m. For Fig. 19(b), the speed is 0.476-(-0.476) = 0.952 m/s and the speed is ±0.476m/s. The acceleration shown in Fig. 19(c) is 17.7-(-11.8) = 29.5m/s^2 and the acceleration is ±14.75m/s^2.

C. SEAT HEIGHT MECHANISM

1) MECHANISM DESIGN

The design of adjustable height region is shown in Fig.1. The height of the seat can be adjusted by the motor, slide rail and ball screw. The all-movable structure for the whole chair is composed of the whole-chair adjustable height structure.

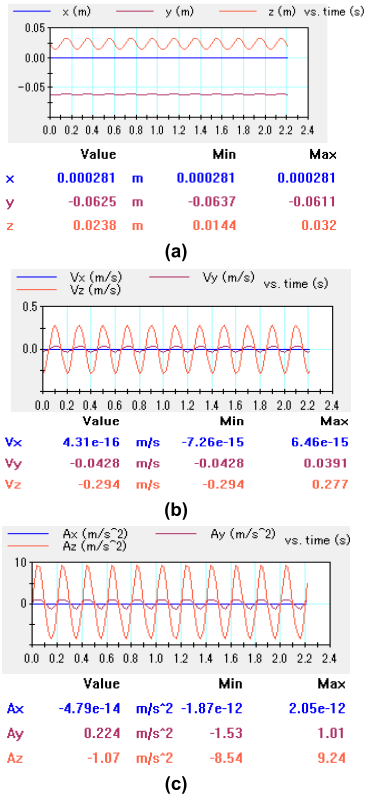

FIGURE 18. Measurement and analysis of the surge axis (a) displacement, (b) velocity and (c) acceleration.

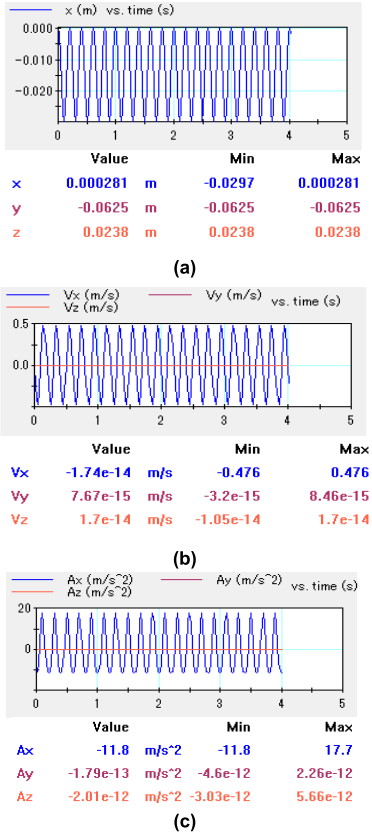

FIGURE 19. Measurement and analysis of the sway axis, (a) displacement, (b) velocity and (c) acceleration.

Therefore, the seat will be pushed by a ball screw-driven platform. The design of the schematic diagram of the mechanism is shown in Fig. 20.

The modeling of the chair is constructed by the Solidworks software. The dimension of the modeling picture is verified dimension through the ANSYS design model. In order to understand the dimension and the FreeCAD, this redraws the solid modeling using the Solidware software. They are shown in Figs. 8-11 and Figs. 14-17. The analytical results of SimWise 4D simulation are shown in Figs. 12-13 and Figs. 18-19.

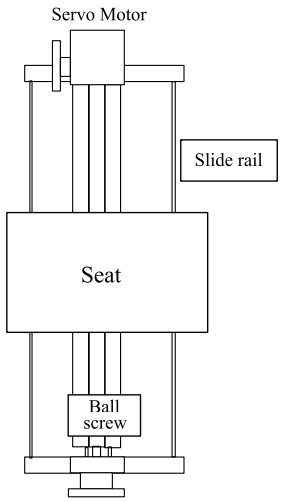

FIGURE 20. Schematic diagram of the seat adjustable height.

IV. IMPLEMENTATION

As implied in Fig. 21, the study has three main aspects, namely: (1) design, analysis, and production of motion chair structures, (2) construction and verification of the inverse kinematic models and (3) establishment of a control box for the motion control system. The motion control system completes the position control and velocity control of the multiaxial motor. Figure 22 shows the flowchart of the implementation. The system is implemented and shown in Figs. 23(a)-(b). The system includes four major parts: the control box, the seat pan, the back pan and the seat height.

The control box contains an industrial computer, five sets of server drivers, the main circuit power supply, and a 24V power. The desktop computer is connected to the six-axis motion control card via a peripheral component interconnect (PCI) express bus. The model of PCI express bus is PCI-1265-AE produced by Advantech. Table 1 shows the expected stroke, and acceleration values for the five movable structures. Table 2 shows the stroke, and acceleration data

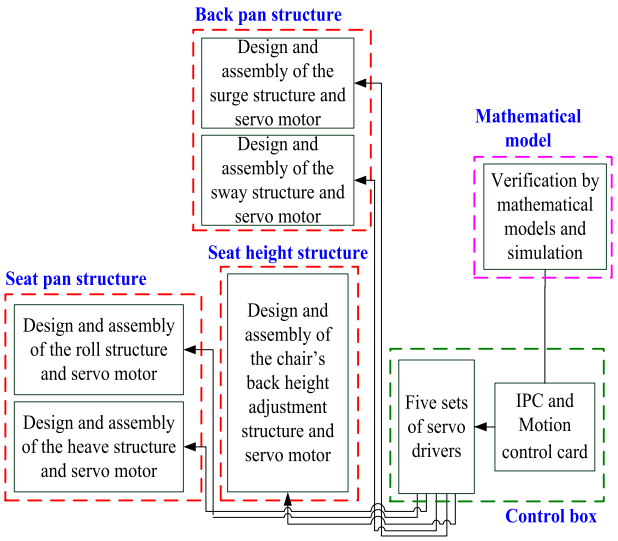

FIGURE 21. The block diagram of the four DoF motion chair.

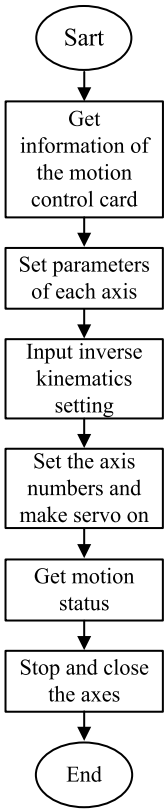

FIGURE 22. Flowchart of the implementation.

obtained from the structure analysis conducted in Section 2. The motor parameters are listed in Table 3.

V. EXPERIMENTAL VALIDATION

The measurement steps for these components and development of the four-axis chair motion system are next described.

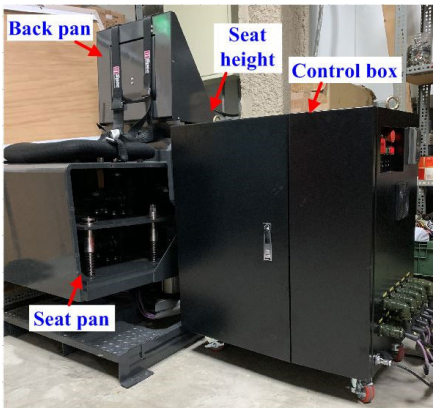

FIGURE 23. The Implemented system, (a) Photography and (b) schematic of wiring between the electric control box and motion chair.

TABLE 1. The expected stroke and acceleration values.

DoF / Item	Surge	Sway	Heave	Roll	Seat height
Stroke (mm)	>± 5	>± 6	>±1	>±15	>± 15
Acceleration (mm/s^2)	>500	>500	>500	>500	>500

TABLE 2. The specifications of the mechanism analysis.

DoF / Item	Surge	Sway	Heave	Roll	Seat height
Stroke (mm)	± 8.8	± 14.88	±3	± 42	± 25
Acceleration (mm/s^2)	8890	14750	2960	50250	2000

For displacement measurement, the total maximum displacement is measured. The used tools are a height gauge, a vernier caliper, and a metal ruler. The measurement reference points of the moveable mechanism are shown in Figs. 24(a)-(f). The measured values for the four DoF and adjustable height conditions are as follows: 43 mm for total surge displacement, 30 mm for total sway displacement, 5.5 mm for total heave displacement, and 79mm for total roll displacement. The

TABLE 3. The parameters of the motor.

DoF / Item	Surge	Sway	Roll	Heave	Seat height
Power dissipation (kW)	0.75	1.3	3.0	3.0	2.0
Rated voltage	220 V	220 V	220 V	220 V	220 V
Rotor inertia (Kg-m^2)	0.00025	0.00201	0.00180	0.00180	0.001214
Rated speed (rpm)	3000	1500	2000	2000	2000
Maximum speed (rpm)	3800	3000	2500	2500	2500
Rated torque (N-m)	2.39	8.34	14.33	14.33	9.55
Maximum torque (N-m)	7.16	23.3	42.69	42.69	28.65
Weight (kg)	3.05	8.9	13.87	13.87	10.16

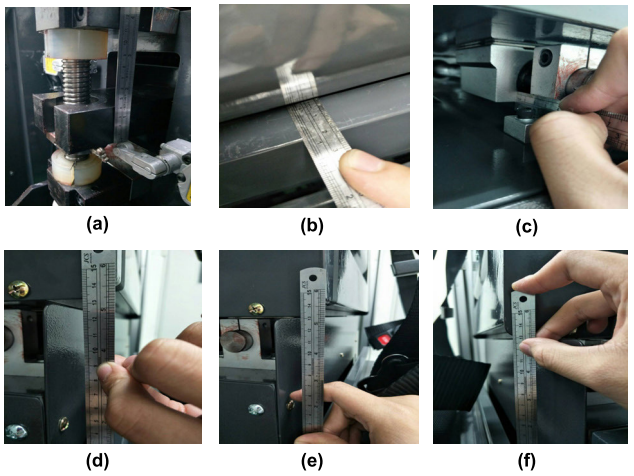

FIGURE 24. The measurement reference point, (a) adjustable height (b) surge axis, (c) sway axis, (d) heave axis, (e) left side of roll axis and (f) right side of roll axis.

model of ball screw used is FSIW-R25-5T4-172-265, and the lead is 5 mm. The total displacement of the adjustable height structure is 55 mm. The pn354 parameter of five drivers is set to 2000, which means the pulse per unit (PPU) is 2000. Starting from zero, the five servo drivers increase the pulse rate by 200, and carry it out 10 times before completing a rotation around the servo motors. The relationships between the motion path of each axis and the pulse rate are shown in Figs. 25(a)-(e). Figures 25(a) and 25(b) show the measured sway-axis and heave-axis errors as the ±0.8mm and ±0.5mm, respectively. Since the structure of the back

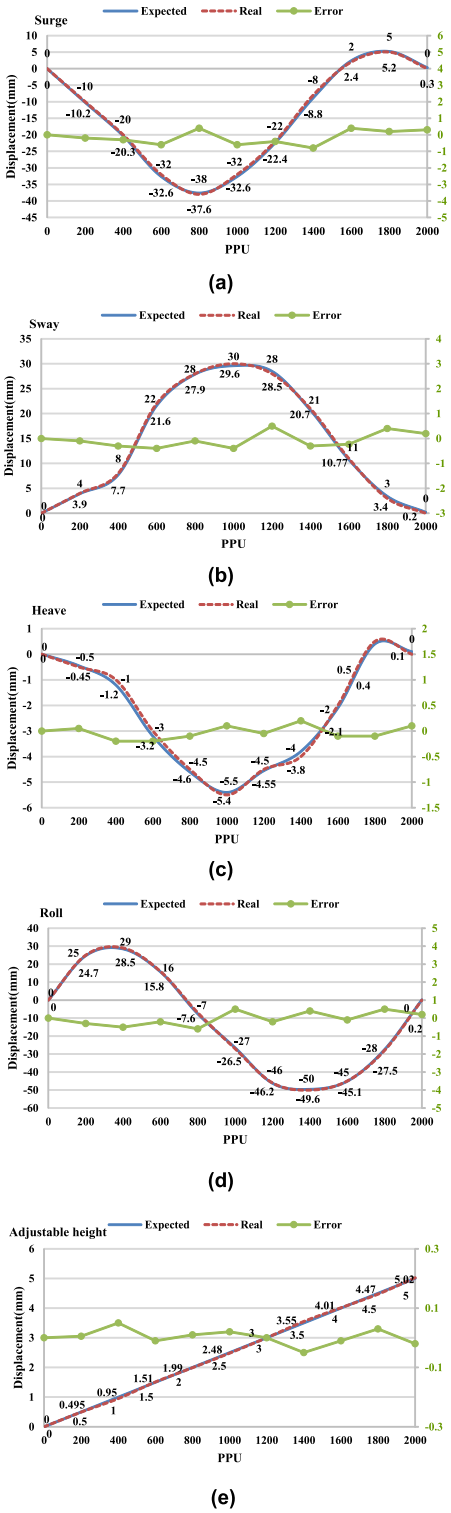

FIGURE 25. The total displacement, (a) surge axis, (b) sway axis, (c) heave axis, (d) roll axis, (e) adjustable height.

pad is a design with a four-link mechanism and a slider crank mechanism, the slight errors occur in the assembly tolerances and links processing. Figure 25(c) shows the measured heave-axis error around ±0.2 mm. The measured result

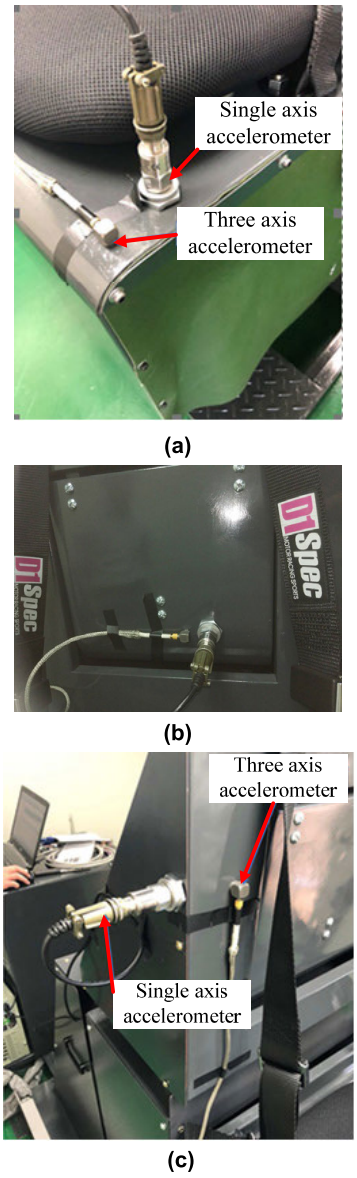

FIGURE 26. The measurement point of acceleration, (a) chair surface (b) surge axis acceleration of the chair's back and (c) sway axis acceleration of the chair's back.

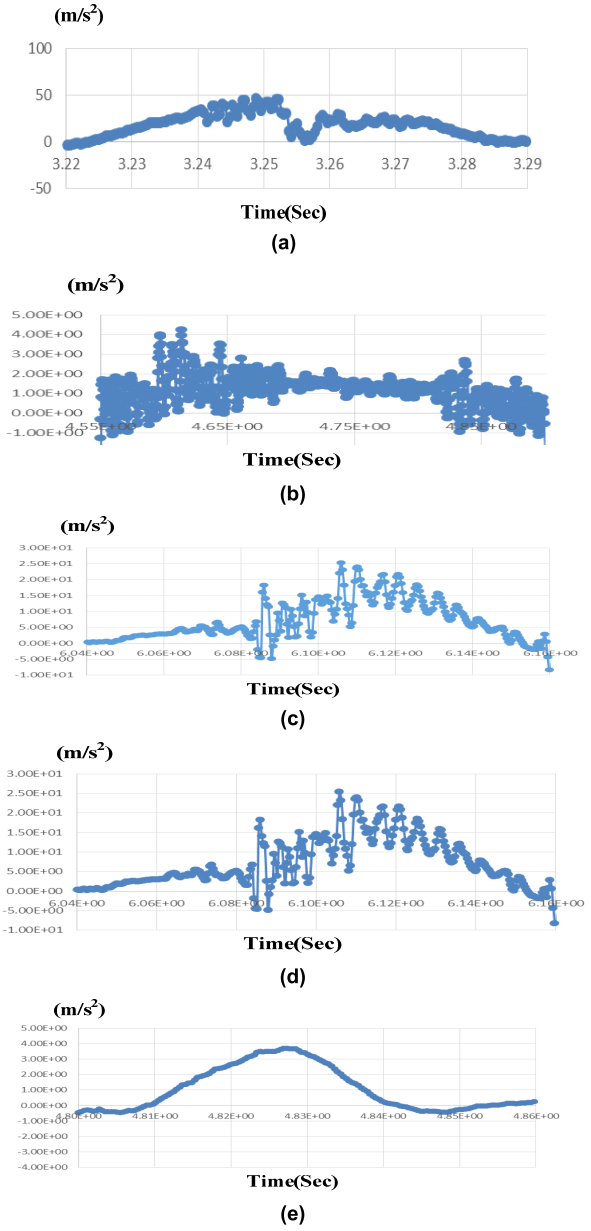

FIGURE 27. The Partial acceleration time domain diagram, a) surge axis, (b) sway axis, (c) heave axis, (d) roll axis and (e) adjustable height.

of the roll axis is shown in Fig. 25(d). The seat plate is the toggle joint structure. Observed from the figure and the seat plate assembly tolerance, it can be seen that the error caused by the installation of the links is about ±0.6mm. Figure 25(e) demonstrates the measured adjustable height structure of the whole chair error around ±0.05mm. The measured displacement of each DoF is close to the expected displacement. Figure 26(a) displays the acceleration measurements of the roll axis, heave axis, and adjustable height using an accelerometer. Figure 26(b) shows the acceleration measurement of the surge axis. The accelerometer is attached to the chair's back for this measurement. Figure 26(c) shows the acceleration measurement of the sway axis motion path. The accelerometer is attached to the support frame on the chair's back for this measurement. Time domain analysis conducted using the accelerometer measurements reveals the changes in acceleration under a fixed rotation speed shown in Figs. 27(a)-(e). Figure 27(a) shows a time domain diagram of the surge axis at the rotational speed of 100 rpm. The maximum acceleration 50.1538 m/s^2 could be achieved under this rotation speed. Figure 27(b) shows a time domain diagram obtained as the sway axis is driven at a rotational speed of 100 rpm. The figure indicates that the maximum acceleration could be 3.88169 m/s^2 at this speed. The heave axis is driven at a rotation speed of 300 rpm, resulting in

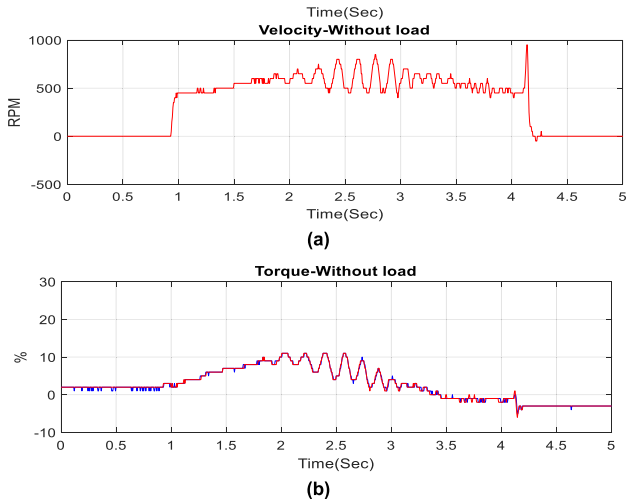

FIGURE 28. The measured results at 500 rpm without load, (a) torque and (b) velocity.

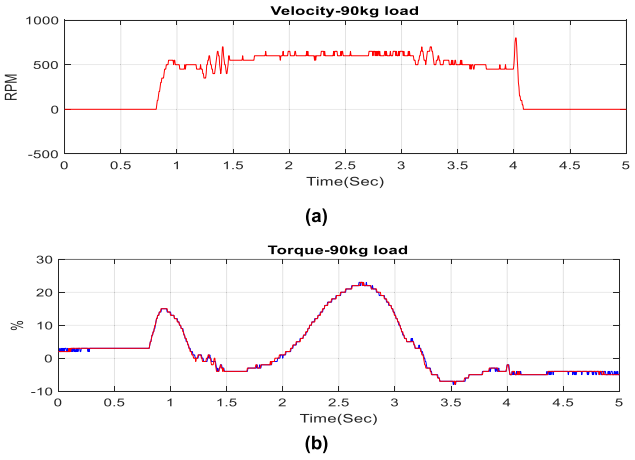

FIGURE 29. The measured results at 500 rpm and 90kg load, (a) torque and (b) velocity.

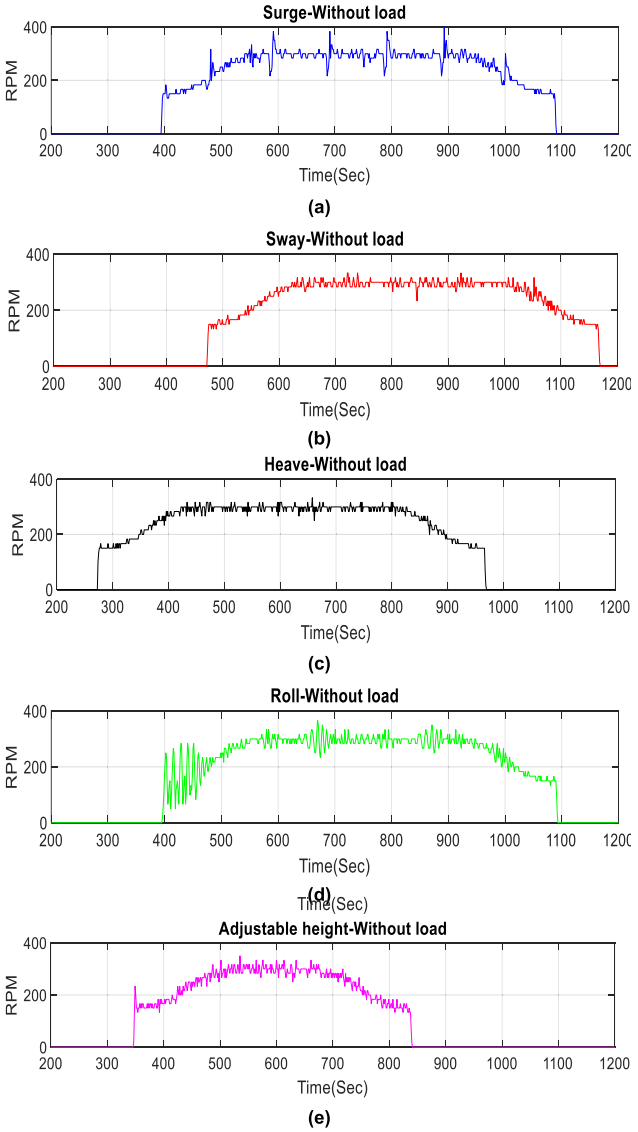

FIGURE 30. The measured results at 300 rpm without load, (a) surge axis, (b) sway axis, (c) heave axis, (d) roll axis and (e) adjustable height.

the time domain diagram in Fig. 27(c), which reveals that the maximum acceleration 24.1206 m/s^2 could be reached. Figure 27(d) is a time domain diagram generated as the servo motor rotates at a speed of 100 rpm. The maximum acceleration could be reached 24.9898 m/s^2 under this condition. Figure 27(e) is a time domain diagram of the adjustable height structure under a rotation speed of 300 rpm. Counting from the starting point of the diagram, the maximum acceleration can be reached 3.49275 m/s^2. Figures 28(a)-(b) and Figures 29(a)-(b) show the responses of the roll axis in torque and rotation speed without and with a load. Under the influence of structure changes and parameter settings, the results indicate that the roll axis is the axis that directly sustains human body weight. Therefore, it is more sensitive to driver parameters. Figures 30(a)–(e) show the T-curve velocity response when the rotation speed is 300 rpm. Figures 31(a)–(e) present the velocity response at 300 rpm after the loading of a 90 kg individual. The figures indicate

TABLE 4. The measurement results.

DoF / Item	Surge	Sway	Heave	Roll	Seat height
Stroke (mm)	±21.5	±15	±2.75	±39.5	±27.5
Acceleration (mm/s^2)	50153.8	3881.69	24120.6	24989.8	3492.75

that that tracking of initiation and stopping on the T-curve is not ideal. The set parameters can be saved to the specified path through the file writing function. Figures 28∼31 show the chair velocity responses, the measurement uses the motion control card to store the relative speed of the servo motor. In the load test, a person weighing 90 kg sits on the seat. Therefore, Figure 29 and Figure 31 mainly measure

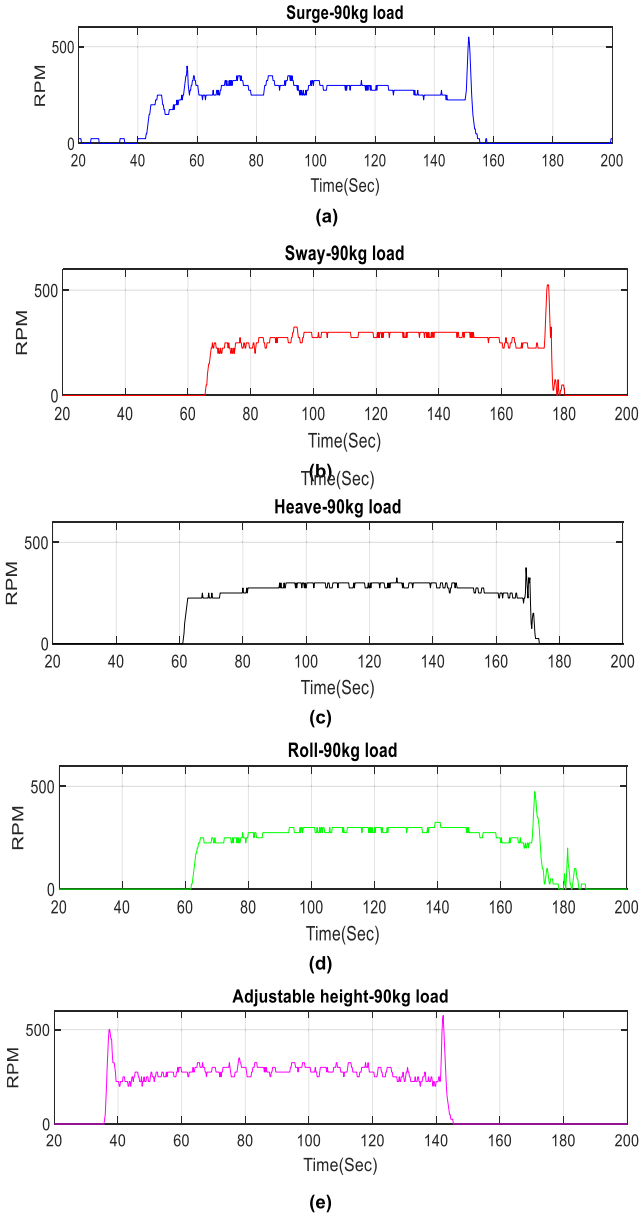

FIGURE 31. The measured results at 300 rpm and 90kg load, (a) surge axis, (b) sway axis, (c) heave axis, (d) roll axis and (e) adjustable height.

the influence of seat startup, transient and steady state on load disturbance. Without modifying the control parameters of the control loop. The reason behind this is that the same controller parameters were used in all the testing sessions. The purpose of using the same parameters is to understand whether the same set of parameters could be used to obtain the expected outcomes under different conditions. Table 4 shows the measurement results.

VI. CONCLUSION

In this paper, a four DoF and adjustable height chair has been discussed. With the aim of achieving the preplanned motion paths and effects, the design, analysis, mathematical model building, simulation, and servo driver establishment for the chair structure are conducted. The target of the study is to develop a structure platform with four DoFs, adjustable height, relevant structure design, mathematical derivation, and software/hardware development. Analysis of different DoFs is performed to gain understanding of the assembly of the structure and further complete its production. Experimental results indicate that the developed chair can approximately sustain a weight of 90 kg. Moreover, the dynamic motion of the chair is simulated and the analytical results include the displacement, velocity and acceleration of the chair. However, the structure strength of the chair is not this main topic of the study that will be considered to evaluate the design in the future work.

REFERENCES

[1] R. Miller, M. Hobday, T. Leroux-Dermers, and X. Olleros, "Innovation in complex systems industries: The case of flight simulation," *Ind. Corporate Change*, vol. 4, no. 2, pp. 363–400, Mar. 1995.
[2] D. Stewart, "A platform with six degrees of freedom," *Proc. Inst. Mech. Eng.*, vol. 180, no. 1, pp. 371–386, 1965.
[3] S. J. Gerathewohl, "Fidelity of simulation and transfer of training: A review of the problem," Federal Aviation Admin., Washington, DC, USA, Office Aviation Med. Rep., 1969.
[4] P. Ji and H. Wu, "A closed-form forward kinematics solution for the 6-6 Stewart platforms," *IEEE Trans. Robot. Autom.*, vol. 17, no. 4, pp. 522–526, Aug. 2001.
[5] H. Lin and J. E. McInroy, "Adaptive sinusoidal disturbance cancellation for precise pointing of Stewart platforms," *IEEE Trans. Control Syst. Technol.*, vol. 11, no. 2, pp. 267–272, Mar. 2003.
[6] D. R. Gum, "Modeling of the human force and motion sensing mechanisms," Air Force Hum. Resoures Lab., Dayton, OH, USA, Tech. Rep. AFHRL-TR-72-54, 1973.
[7] F. M. Cardullo, "Advanced G seat for aircraft simulation," U.S. Patent 3 983 640, Oct. 15, 1976.
[8] D. R. Berger, J. Schulte-Pelkum, and H. H. Bálthoff, "Simulating believable forward accelerations on a Stewart motion platform," *ACM Trans. Appl. Perception*, vol. 7, no. 1, pp. 1–27, Jan. 2010.
[9] M. Bruschetta, Y. Chen, D. Cunico, E. Mion, and A. Beghi, "A nonlinear MPC based motion cueing strategy for a high performance driving simulator with active seat," in *Proc. AMC*, Mar. 2018, pp. 23–28.
[10] Y. Toda, K. Asano, K. Yamamoto, F. Yamamoto, S. Hayakawa, S. Tsutsumi, R. Ikeura, T. Yamakawa, M. Yoshida, T. Tsutsui, and H. Tobata, "Verification of reducing effect of driver fatigue increase by using the driver's seat with two support mechanisms," in *Proc. ROBIO*, Dec. 2018, pp. 1569–1573.
[11] Y. Ishii, T. Ikeda, T. Kobayashi, Y. O. Kato, A. Utsumi, I. Nagasawa, and S. Iwaki, "Investigation of the driver's seat that displays future vehicle motion," in *Proc. ROMAN*, Dec. 2019, pp. 1–6.
[12] R. Halicioglu, L. C. Dülger, and A. T. Bozdana, "An automation system for data processing and motion generation," in *Proc. Int. Artif. Intell. Data Process. Symp.*, Malatya, Turkey, Sep. 2017, pp. 1–9.
[13] K. S. Fu, R. C. Gonzalez, and C. S. G. Lee, *Robotics Control, Sensing, Vision, and Intelligence*. New York, NY, USA: McGraw-Hill, 1987.
[14] F. Wang, Z. Qian, Z. Yan, C. Yuan, and W. Zhang, "A novel resilient robot: Kinematic analysis and experimentation," *IEEE Access*, vol. 8, pp. 2885–2892, 2020.
[15] J. Zhang, H. Wei, Y. Shan, P. Li, Y. Zhao, L. Qi, and H. Yu, "Modeling and experimental study of a novel multi-DOF parallel soft robot," *IEEE Access*, vol. 8, pp. 62932–62942, 2020.
[16] H. H. Mabie, and C. F. Reinholtz, *Mechanisms and Dynamics of Machinery*. New York, NY, USA: Wiley, 1987.
[17] R. Halicioglu, L. C. Dulger, and A. T. Bozdana, "Modeling, design, and implementation of a servo press for metal-forming application," *Int. J. Adv. Manuf. Technol.*, vol. 91, nos. 5–8, pp. 2689–2700, 2017.
[18] I. Cvok, M. Hrgetić, M. Hoić, J. Deur, and V. Ivanovic, "Design of a linear motor-based shaker rig for testing driver's perceived ride comfort," *Mechatronics*, vol. 75, May 2021, Art. no. 102521.
[19] (2005). *SimWise 4D Motion Simulation, Stress Analysis, and Optimization*. [Online]. Available: https://www.design-simulation.com/SimWise4d/

MING-YEN WEI was born in Taichung, Taiwan, in April 1983. He received the B.S. and M.S. degrees in electrical engineering from the National Formosa University, in 2005 and 2007, respectively, and the Ph.D. degree in electrical engineering from the National Taiwan University of Science and Technology, Taipei, Taiwan, in 2012. Since 2012, he has been a Faculty Member with the Aeronautical System Research Division, Simulation System Section, National Chung-Shan Institute of Science and Technology. His research interests include mechatronics, motor drive control, control applications, and platform design.

YEN-LIANG YEH was born in Kaohsiung, Taiwan, in October 1972. He received the B.S. degree from Far East University, in 1992, the M.S. degree from the National Taiwan University of Science and Technology, in 1998, and the Ph.D. degree from the National Cheng Kung University, in 2001, all in mechanical engineering. He has been a Professor with the Department of Mechanical Engineering, National Chin-Yi University of Technology. His research interests include mechanical, CAE, structure analysis, optical measurement, and nonlinear dynamic.

SHIAW-WU CHEN was born in Kaohsiung, Taiwan, in April 1959. He received the B.S. degree in mechanical engineering from Tamkang University, in 1979, and the M.S. and Ph.D. degrees in mechanical engineering from the University of California, Los Angeles. He has been an Associate Professor with the Department of Automatic Control Engineering, Feng Chia University. His research interests include servo control, adaptive signal processing, and digital signal processing.

HSIU-MING WU received the Ph.D. degree from the Department of Electrical Engineering, National Taiwan University of Science and Technology, in 2009. Next, he served the Opto-Mechatronics Technology center, National Taiwan University of Technology as a Postdoctoral Fellow, for three years. In early 2013, he worked with Texas A&M University at Qatar as a Postdoctoral Fellow, for four years. In early 2018, he joined the Department of Mechanical Engineering at the National Chin-Yi University of Technology, Taichung, for two years. He is currently an Assistant Professor with the Department of Intelligent Automation Engineering, National Taipei University of Technology. His research interests include mechatronics, nonlinear control, and robotic control.

JI-WEI LIU was born in Taichung, Taiwan, in November 1991. He received the B.S. degree in electronic engineering from the National Chin-Yi University of Technology, in 2017. Since 2018, he has been a Technician with the Aeronautical System Research Division, Simulation System Section, National Chung-Shan Institute of Science and Technology. His research interest includes electric control.